In-Situ Characterization of the Uncrimping Process of Arterial Collagen Fibers Using Two-Photon Confocal Microscopy and Digital Image Correlation

Ruoya Wang[1,4], **Luke P. Brewster**[3,4,5], and **Rudolph L. Gleason Jr.**[1,2,3]

[1]George W. Woodruff School of Mechanical Engineering, Georgia Institute of Technology, Atlanta, GA, USA

[2]Wallace H. Coulter Department of Biomedical Engineering, Georgia Institute of Technology, Atlanta, GA, USA

[3]Parker H. Petit Institute of Bioengineering and Bioscience, Georgia Institute of Technology, Atlanta, GA, USA

[4]Department of Surgery, Division of Vascular Surgery, Emory University School of Medicine, Atlanta, GA, USA

[5]Atlanta VA Medical Center, United States Department of Veterans Affairs, Atlanta, GA, USA

Abstract

Uncrimping of collagen fibers in the arterial wall is an integral process in modulating the macro-level mechanical response of arteries. Uncrimping of collagen fibers leads to a gradual, but significant strain-stiffening response of the artery at physiological pressures and prevents overdistention at elevated pressures. In this study, we imaged adventitial collagen fibers from a fresh primate artery using two-photon excitation microscopy while subjecting the artery to physiological inflation pressures and axial stretch. The imaging focal plane was fixed at a constant radial location in the adventitial wall by adjusting the focal distance as the artery inflated, allowing for the continuously monitoring of the uncrimping process of a single region of collagen fibers. Digital image correlation was then applied to the sequential images to assess and correlate the local displacements to manual traces of selected reference fibers and their engagements. We found that the collagen fibers of interest became fully engaged at a luminal pressure of 20 mmHg, this was then followed by significant rotation of these fibers as the bulk artery continued to dilate. This technique allows for the development of uncrimping metrics to more accurately characterize the

Corresponding Author: Roy Wang, Department of Vascular Surgery, Emory University School of Medicine, 101 Woodruff Circle, 5211 WMB, Atlanta, GA 30322, USA, r.wang@gatech.edu, Phone: (404) 727-8329, Fax: (404) 727-3660.

Conflict of interest statement

There are no conflicts of interest.

kinematics of collagen fibers under physiological loads, which can aid in the development of more accurate microstructural constitutive models for arteries.

Keywords

adventitia; digital image correlation; two-photon excitation microscopy; deformation; arterial mechanics

1. Introduction

Collagen fibers (CFs) are considered the primary load-bearing constituent in the arterial wall. The high tensile strength of CFs and their abundance, particularly in the adventitia, provide structural support and prevent the overdistention of the arterial wall at elevated blood pressures (Holzapfel, et al. 2000). However, at sub-physiological pressures, CFs are undulated or crimped, and therefore present minimal resistance to loading. As the arterial wall dilates with increasing luminal pressure, the undulated CFs uncrimp and become engaged (i.e. straightened), and this process results in significant strain-stiffening and loading resistance of the wall (Cox 1978). The uncrimping process of CFs is an integral component of the non-linear mechanical response of arteries. The kinematics of the uncrimping is complex and not well understood, and a better understanding of this process can help in the formulation of more physiologically relevant microstructurally-motivated constitutive models (Cacho, et al. 2007, Gasser, et al. 2012).

This study presents a proof-of-concept utilizing digital image correlation (DIC) and two-photon excitation microscopy (TPEM) techniques to characterize the uncrimping process of adventitial collagen fibers in the cylindrical configuration of arteries subjected to physiological pressures and axial stretches. The second harmonic generation (SHG) signals of the CFs were used as natural stochastic patterns for the DIC analysis. The uncrimping process in each artery was assessed across a fixed area and radial location, thus allowing for the continuous tracking of the same group of CFs across the entire pressure-loading regime. We found that the sampled CFs became fully uncrimped and engaged prior to the onset of significant strain-stiffening in the wall. This result was in agreement with manual traces of selected individual fibers in the same region of interest. Lastly, we characterized the mean displacement directions of the CFs with loading.

2. Methods

2.1 Mechanical Testing

Two common carotid arteries (one right and one left) were harvested from two healthy non-human primates (rhesus macaques) during necropsy. The ages of the animals and the traction-free geometries of the respective arteries are provided in Table 1.

The arteries were flushed immediately with saline and transported on iced saline to the laboratory. Adherent perivascular tissues were carefully removed by sharp dissection and the arteries were cannulated on a cylindrical biaxial mechanical testing device; similar devices are described in detail elsewhere (Gleason, et al. 2004, Zaucha, et al. 2009). The

arteries were subjected to cyclic, quasi-static constant rate pressurizations between 0 and 120 mmHg at fixed axial lengths while their outer diameters and axial forces were recorded in-line. During testing, the arteries were continuously submerged in a Ca^{2+} and Mg^{2+}-free Dulbecco's phosphate-buffered saline (DPBS, Corning Cellgro) bath maintained at 37 °C. Axial lengths were incrementally increased and the arteries were preconditioned at each increment by several pressurization cycles to achieve repeatable pressure-diameter curves. Based on established methods, the axial lengths in which the axial forces ceased to vary with pressure was deemed to be the in-vivo axial lengths of the arteries (Van Loon 1977). Once this configuration was established, the arteries were transferred to a secondary cylindrical biaxial device designed to fit on an inverted multi-photon confocal microscope (LSM 510 META NLO, Zeiss) for TPEM analysis of the CFs.

2.2 Multiphoton Imaging

The arteries were axially stretched prior to imaging to their pre-determined in-vivo axial lengths and preconditioned again with several pressurization cycles to ensure repeatability. The arteries were then pressurized from 0 mmHg in a stepwise manner by 5 mmHg increments to 50 mmHg and then by 10 mmHg increments to 120 mmHg. This pressurization scheme was implemented to ensure small deformations needed to perform the DIC analysis. At each pressure increment, the arteries were excited with an 800 nm laser and the SHG signals of the CFs were collected through a 380–420 nm bandpass filter using a 20X objective (Wan, et al. 2010). Each frame was averaged 16 times to maximize the resolution. To maintain the same region of interest, the focal plane of the microscope objective was fixed at a single radial location through manual adjustments of the focal distance as the arteries inflated. CFs in the focal plane that could be uniquely tracked by visual observation throughout the entire pressurization ramp were used as references for the manual adjustments. Several areas on the arteries were sampled prior to the final imaging sequence in order to identify an appropriate set of reference CFs; the final regions of interest were located approximately in the center of the arteries at a depth of 20–30 μm into the arterial wall.

2.3 DIC Analysis

DIC was performed between sequential images using a modified open source algorithm (OpenPIV) in MATLAB (Taylor, et al. 2010). The algorithm was tested on a representative pair of identical SHG images of CFs in which one of the images was translated by 30 pixels at 45 degrees. Furthermore, the percent engagement of three reference fibers in artery 1 was measured by manually tracing the fiber lengths using ImageJ (National Institute of Health), see Fig. 1A–B. The engagement percentage was defined as the percent ratio of the fiber's chord length (straight line end-to-end) to total length, thus 100% engagement denoted a fully engaged, straightened fiber. DIC results, either magnitude or direction of the displacement vectors, are presented as the mean ± standard deviation across the entire region of interest.

3. Results

The in-vivo axial stretch ratios (the ratio of the in-vivo length to traction-free length) were determined to be $\lambda_z = 1.35$ and 1.50 for arteries 1 and 2, respectively. DIC performed on the

translated identical image pair yielded a mean displacement of 31.2 ± 0.84 pixels and an angle of 46.1 ± 5.2 degrees, in close agreement with the prescribed translation of 30 pixels at 45 degrees. The deviation from the prescribed translation was likely due to the lack of unique stochastic patterns in small dark regions inherent to SHG images in which the DIC algorithm was unable to cross-correlate. The interrogation window size was optimized to minimize this effect. Sequential SHG images of the CFs were captured at the arteries' in-vivo axial stretches (Fig. 1C–D, see supplemental videos). The magnitudes of the displacement vectors decreased significantly to a nearly homogeneous level once the CFs became fully engaged (Fig. 1C–D magnified boxes). The three reference fibers manually traced reached nearly 100% engagement at 20 mmHg (Fig. 2). Similarly, DIC analysis showed an appreciable decrease in the mean displacement for both arteries around 20 mmHg (Fig. 3). For artery 1, linear regression between the mean engagement percentage and mean DIC displacement yielded high correlation (goodness-of-fit $R^2 = 0.961$). For artery 2, we observed large rigid body motions in the CFs following the increase in loading increment from 5 to 10 mmHg that was implemented at 50 mmHg. These motions, which are evident in the supplemental video for artery 2, resulted in large spurious displacement vectors following the DIC analysis. To correct this issue, we excluded displacement magnitudes that were more than one standard deviation greater than the averaged mean $\pm$ standard deviation of the last three 5 mmHg increment loading points (i.e. 35–40 mmHg, 40–45 mmHg, and 45–50 mmHg).

The fiber displacement directions (FDD) were calculated using circular statistics (Fisher 1995) implemented through the Circular Statistics Toolbox in MATLAB. For artery 1, we found that the FDD appeared more circumferential (0 deg) at low pressures, in agreement with the circumferential dilation of the artery, but became more axially dominated (+/− 90 deg) as pressure increased beyond the CF engagement point (Fig. 4–5). The FDD differential with loading was more significant in artery 2. Note that the drop in the FDD in artery 2 at 45 mmHg corresponds to the increase in loading increment. Be mindful that the displacement direction of the CFs described in this analysis does not indicate the fiber orientation.

4. Discussion

To our knowledge, this study is the first to characterize the uncrimping process of CFs from an artery in the cylindrical geometric configuration subjected to physiological loading conditions. The CFs were imaged at fixed radial locations with pressurization using TPEM. Fixing radial location allowed the same region of interest to be assessed as the artery was pressurized. DIC was used to provide area-based characterization of the uncrimping dynamics through analysis of the local displacement vectors. Interestingly, the CFs appeared to become fully engaged prior to the onset of significant strain stiffening. Furthermore, we found that following engagement, the CFs exhibited significant rotation as the bulk artery continued to dilate. We speculate that CFs exhibit transmural differences in engagement thresholds, with CFs deeper in the wall having a higher engagement pressure than ones located further outward. As a result, the CFs that were engaged earlier in the loading regime were forced to rotate in order for the artery to continue to dilate without damaging the engaged fibers. However, this rotation may also be due to a predominately cross-fiber

displacement direction during uncrimping of the CFs which transitions to an axial displacement once the fibers are engaged. It would be of interest in future studies to decouple bulk fiber rotations from cross-fiber displacements to better understand the underlying mechanisms of CF kinematics.

As a proof-of-concept study, several limitations need to be addressed in order to evaluate the findings and help refine future studies. First, attenuation of SHG in dense biological tissues, such as the arterial wall, prevents imaging CFs across the entire wall of medium to large arteries. Healthy primate arteries were utilized for physiological relevance, but future studies may include imaging smaller arteries, such as ones from mice, where the SHG signal can be observed through the entire wall. This will allow for the validation of transmural differences in the engagement thresholds of CFs. Second, this study assumed a two-dimensional deformation field of the CFs, since DIC was applied to planar images. However, inflation of a cylindrical tube is inherently a three-dimensional process, and this difference will need to be better characterized. Using a high magnification objective may minimize the curvature effect of the artery. We emphasize that both sufficient resolution in the TPEM images as well as small displacements between loading points are needed in order to successfully implement this technique. This requirement is best demonstrated in the measurements of artery 1, while both the resolution and loading increments were less than optimal in artery 2. Despite this, the salient responses were still captured in artery 2. Lastly, we only examined the uncrimping behavior with increasing pressure at a fixed axial stretch. It would be of interest in future studies to examine the uncrimping process as the artery is axially stretched as well as the uncrimping and crimping process during inflation and deflation cycles in order to elucidate the mechanisms of hysteresis.

Supplementary Material

Refer to Web version on PubMed Central for supplementary material.

Acknowledgments

References

Cacho F, Elbischger P, Rodriguez J, Doblare M, Holzapfel GA. A constitutive model for fibrous tissues considering collagen fiber crimp. International Journal of Non-Linear Mechanics. 2007; 42:391–402.

Cox RH. Passive mechanics and connective tissue composition of canine arteries. American Journal of Physiology-Heart and Circulatory Physiology. 1978; 234:H533–H541.

Fisher, NI. Statistical analysis of circular data. Cambridge University Press; 1995.

Gasser TC, Gallinetti S, Xing X, Forsell C, Swedenborg J, Roy J. Spatial orientation of collagen fibers in the abdominal aortic aneurysm's wall and its relation to wall mechanics. Acta Biomaterialia. 2012

Gleason R, Gray S, Wilson E, Humphrey J. A multiaxial computer-controlled organ culture and biomechanical device for mouse carotid arteries. Journal of Biomechanical Engineering. 2004; 126:787–795. [PubMed: 15796337]

Holzapfel G, Gasser T, Ogden R. A new constitutive framework for arterial wall mechanics and a comparative study of material models. Journal of Elasticity. 2000; 61:1–48.

Taylor ZJ, Gurka R, Kopp GA, Liberzon A. Long-duration time-resolved PIV to study unsteady aerodynamics. Instrumentation and Measurement, IEEE Transactions on. 2010; 59:3262–3269.

Van Loon P. Length-force and volume-pressure relationships of arteries. Biorheology. 1977; 14:181–201. [PubMed: 912047]

Wan W, Yanagisawa H, Gleason RL Jr. Biomechanical and microstructural properties of common carotid arteries from fibulin-5 null mice. Annals of Biomedical Engineering. 2010; 38:3605–3617. [PubMed: 20614245]

Zaucha MT, Raykin J, Wan W, Gauvin R, Auger FA, Germain L, Michaels TE, Gleason RL Jr. A novel cylindrical biaxial computer-controlled bioreactor and biomechanical testing device for vascular tissue engineering. Tissue Engineering Part A. 2009; 15:3331–3340. [PubMed: 19385725]
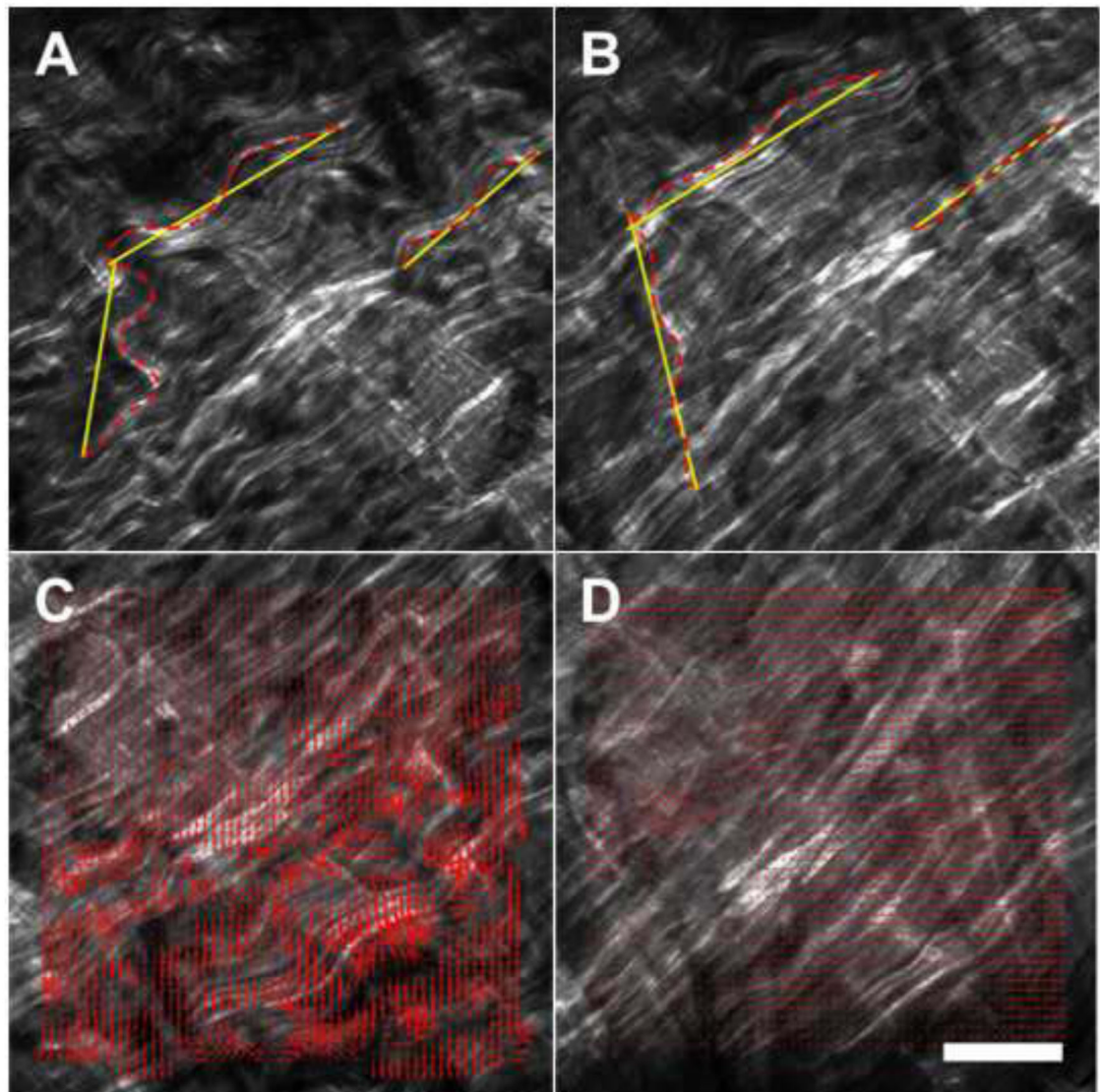
Fig. 1.
Three reference fibers manually traced at low pressure (A) and high pressure (B). Dashed lines denote the fiber chord lengths while solid lines are the total fiber lengths. The engagements of the fibers are calculated as percent ratios of these two lengths. Corresponding DIC displacement vectors for low (C) and high pressures (D). Note that the displacement magnitudes decrease significantly for the high pressure. White scale bar ≈ 100 μm.
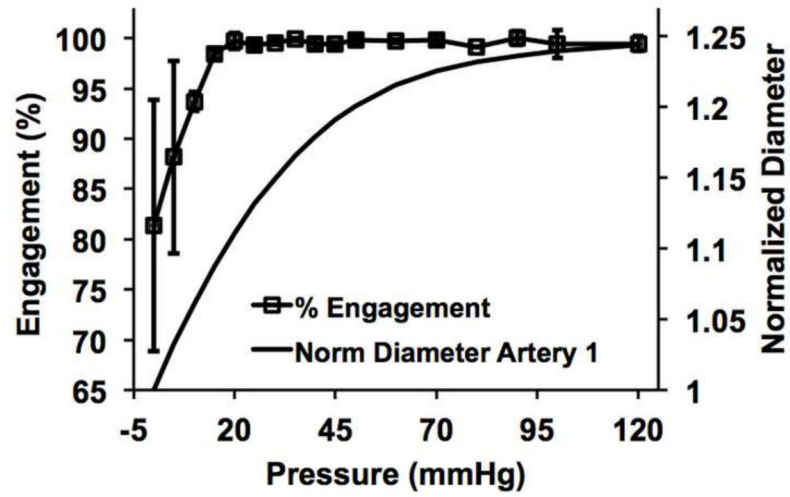
Fig. 2.
Percent of engagement with pressure calculated from the manual traces of the three reference fibers. These fibers reached nearly 100% engagement by 20 mmHg of luminal pressure.
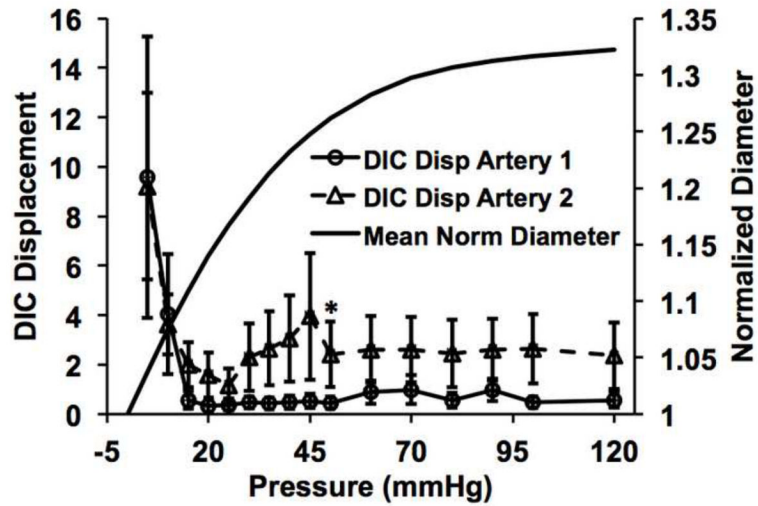
Fig. 3.
Mean DIC displacement with pressure showing an appreciable decrease in displacement magnitude that corresponds to the 100% engagement pressure point in Fig. 2. Both percent engagement and DIC results are plotted with the mean pressure-diameter responses of the arteries. Note that the collagen fibers appear to become fully engaged prior to significant strain-stiffening of the wall. The asterik indicates the point from which the outlier correction was applied (see Methods section).
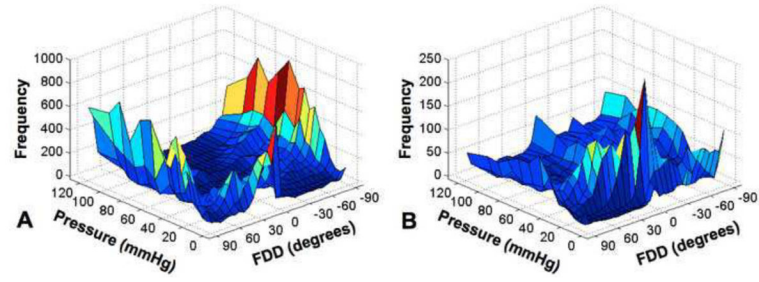
Fig. 4.
Three-dimensional histogram heatmaps of the FDD (Fiber Displacement Direction) with pressure of arteries 1 and 2. 0 and 90 degrees correspond to the circumferential and axial directions of the artery, respectively.
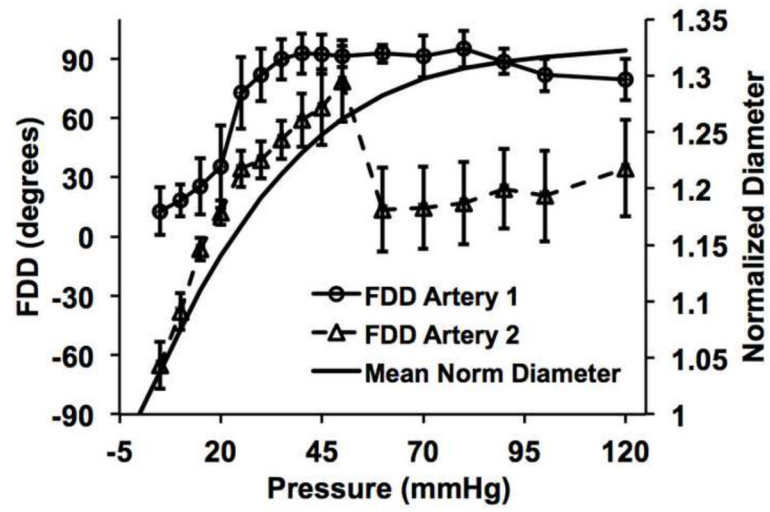
Fig. 5.
Circular mean analysis of the FDD across the entire region of interest. Both arteries exhibit similar rotational responses. Artery 2 appears to undergo greater roation than artery 1.

Table 1

Specimen age and traction-free geometries of arteries used in this study.

	Type	Age	Outer Diameter	Wall Thickness	Length
Artery 1	RCCA	7 yrs	3.10 mm	0.46 mm	13.0 mm
Artery 2	LCCA	2 yrs	2.74 mm	0.58 mm	19.6 mm

RCCA: Right Common Carotid Artery, LCCA: Left Common Carotid Artery